Electronic Supplementary Information

Anisotropic Electrene T′-Ca_2P with Electron Gas Magnetic Coupling as Anode Material for Na/K Ion Batteries

Jiaxin Jiang,[a,†] Kai Wang,[a,†] Hongyan Guo,[a] Guizhong Zuo,[b] Zhiwen Zhuo,[*a] and Ning Lu[*a]

[a]Anhui Province Key Laboratory of Optoelectric Materials Science and Technology, Key Laboratory of Functional Molecular Solids Ministry of Education, and Department of Physics, Anhui Normal University, Wuhu, Anhui 241000, China

[b]Institute of plasma physics, HIPS, Chinese academy of Sciences, Hefei, 230031, China

*Corresponding authors: Zhiwen Zhuo, E-mail: zhuozw@ahnu.edu.cn, Anhui Normal University, Wuhu, Anhui 241000, China

Ning Lu, E-mail: luning@ahnu.edu.cn, Anhui Normal University, Wuhu, Anhui 241000, China

I. Structure information of T-Ca_2P and T′-Ca_2P

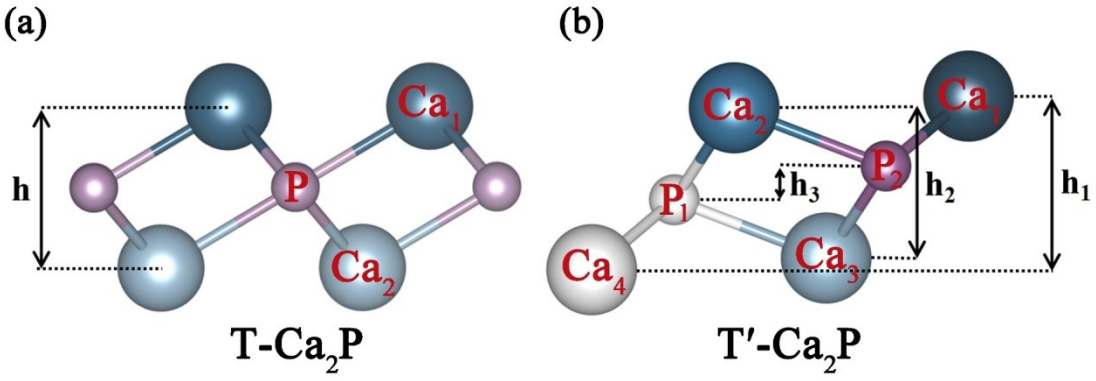

Fig. S1 Side view of T-Ca_2P (a) and T′-Ca_2P (b) structure.

Table S1 Structural information of T-Ca_2P, FM, AFM-0D, AFM-1D_1 and AFM-1D_2 T′-Ca_2P.

Phase	Space Group	Lattice Constants (Å)	Bond Length (Å)	Bond Angle (°)
T-Ca_2P	P-3m1	a = 4.23 h = 2.90	d_{Ca-P} = 2.83	Ca-P-Ca = 83.92 P-Ca-P = 96.08
FM T′-Ca_2P	P21/m	a = 7.38 b = 4.23 h_1 = 3.00 h_2 = 2.60 h_3 = 0.58	d_{Ca1-P1} = 2.84 d_{Ca2-P1} = 2.82 d_{Ca3-P1} = 2.85	Ca_1-P_2-Ca_2 = 108.68 Ca_2-P_1-Ca_3 = 81.88 Ca_1-P_2-Ca_3 = 81.95 P_1-Ca_2-P_2 = 98.12
AFM-0D T′-Ca_2P	P21/m	a = 7.35 b = 8.41 h_1 = 3.07 h_2 = 2.66 h_3 = 0.58	d_{Ca1-P1} = 2.89 d_{Ca2-P1} = 2.86 d_{Ca3-P1} = 2.83	Ca_1-P_2-Ca_2 = 107.62 Ca_2-P_1-Ca_3 = 82.01 Ca_1-P_2-Ca_3 = 83.61 P_1-Ca_2-P_2 = 97.99
AFM-1D_1 T′-Ca_2P	P21/m	a = 7.38 b = 4.26 h_1 = 2.99 h_2 = 2.57 h_3 = 0.62	d_{Ca1-P1} = 2.89 d_{Ca2-P1} = 2.85 d_{Ca3-P1} = 2.83	Ca_1-P_2-Ca_2 = 109.56 Ca_2-P_1-Ca_3 = 81.71 Ca_1-P_2-Ca_3 =81.82 P_1-Ca_2-P_2 = 98.29
AFM-1D_2 T′-Ca_2P	P21/m	a = 14.75 b = 4.23 h_1 = 3.04 h_2 = 2.62 h_3 = 0.58	d_{Ca1-P1} = 2.89 d_{Ca2-P1} = 2.85 d_{Ca3-P1} = 2.83	Ca_1-P_2-Ca_2 = 108.35 Ca_2-P_1-Ca_3 = 82.01 Ca_1-P_2-Ca_3 = 82.85 P_1-Ca_2-P_2 = 97.99

II. The details of magnetic coupling

Three different magnetic coupling in the T′-Ca_2P are considered here: (I) inner-channel coupling; (II) inter-channel coupling on same surface and (III) inter-channel coupling on different surfaces. Three different AFM configurations have been investigated, as shown in Fig. S2†. Among the exchange interactions, the coupling I is direct exchange interaction, coupling II and III are indirect exchange interaction. Our results indicate that the coupling I is strong while coupling II and III are quite weak. There is relatively strong *d*(Ca)-*d*(Ca) coupling within AFM interaction for coupling I, due to the too close distance between magnetic LAE. For the coupling II, there is much weaker *d*(Ca)-*d*(Ca) coupling within FM interaction based on the energy difference between FM and AFM-$1D_2$, when the distance between magnetic LAE is significantly large. For the coupling III, there is weakest *d*(Ca)-*p*(P)-*d*(Ca) indirect coupling between the magnetic LAE, that the energy difference between FM and AFM-$1D_1$ is quite close.

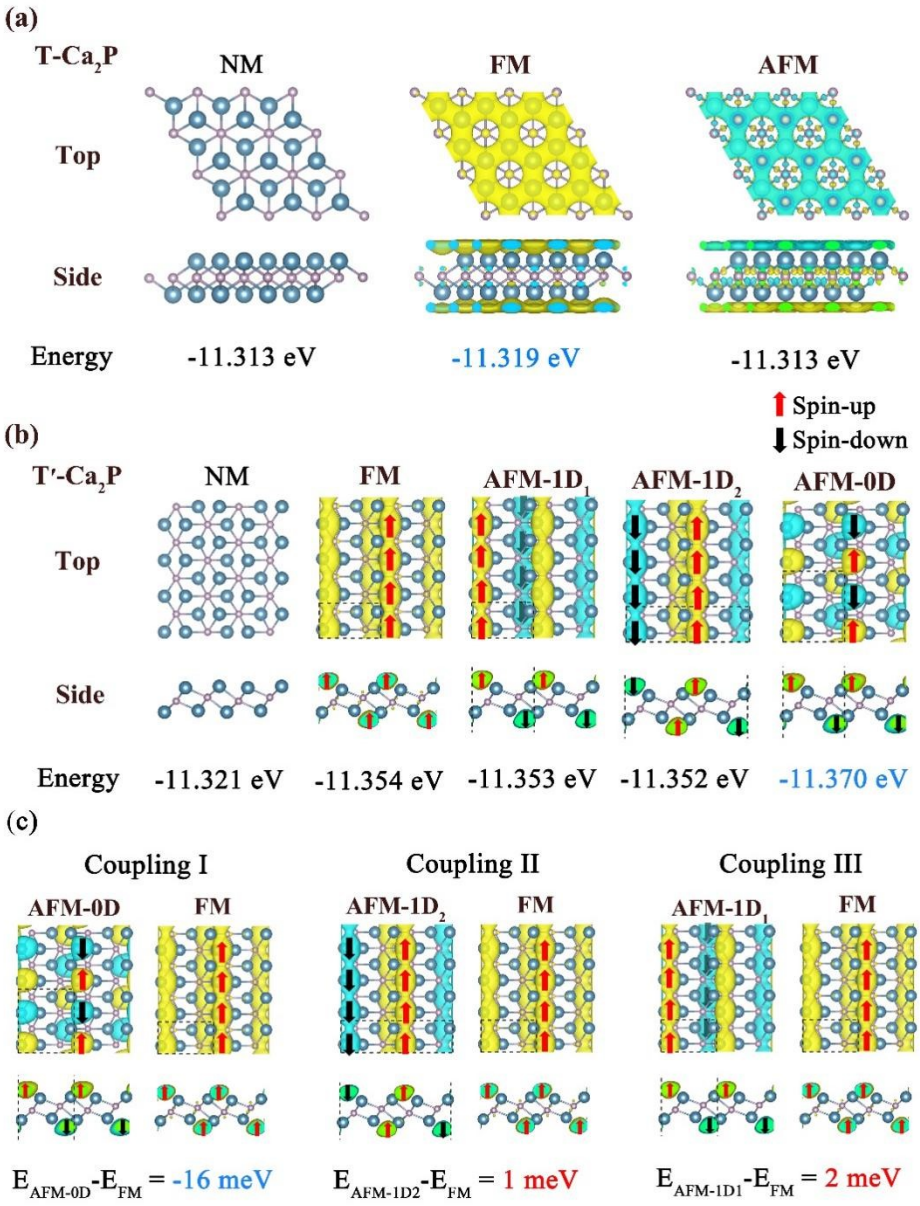

Fig. S2 The spin charge density and energy of unit formula cell (Ca_2P) of T-Ca_2P (a) and T′-Ca_2P (b) at different magnetic states, including: NM, FM and AFM T-Ca_2P; NM, FM, AFM-$1D_1$, AFM-$1D_2$ and AFM-0D T′-Ca_2P. (c) Schematic diagram of three different magnetic coupling and the energy difference between corresponding magnetic states and FM. Isovalue of 0.002 e/Bohr^3.

III. The structure stabilities of T′-Ca_2P monolayer

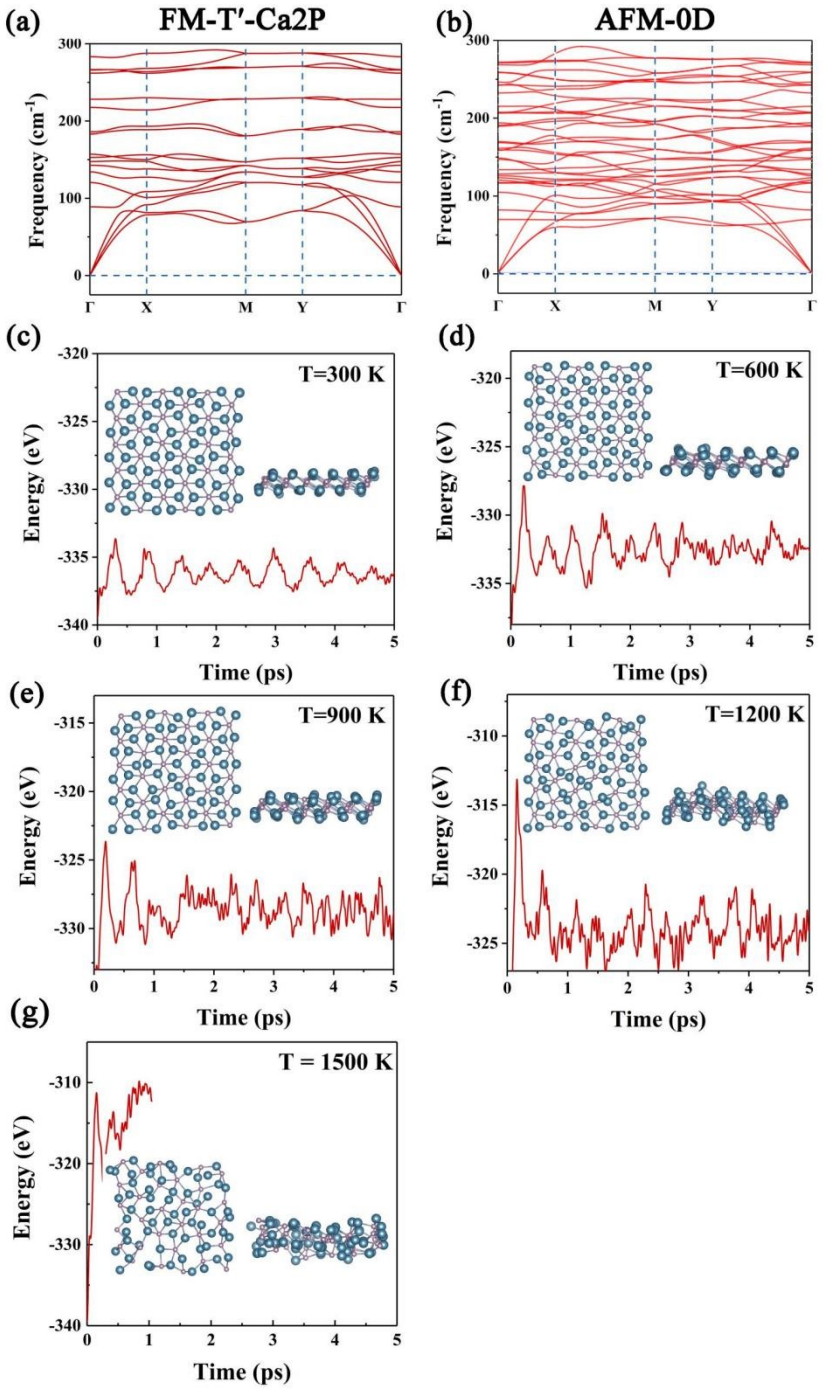

Fig. S3 The phonon dispersion of (a) FM and (b) AFM-0D T′-Ca_2P monolayer. Changes of total energy in AIMD simulations at 300 K (c), 600 K (d), 900 K (e), 1200 K (f) and 1500 K (g); inserted correspond snapshots of T′-Ca_2P (3×5 supercell) at the end of AIMD simulations.

IV. Electronic properties of NM, FM and AFM of T and T′ phases

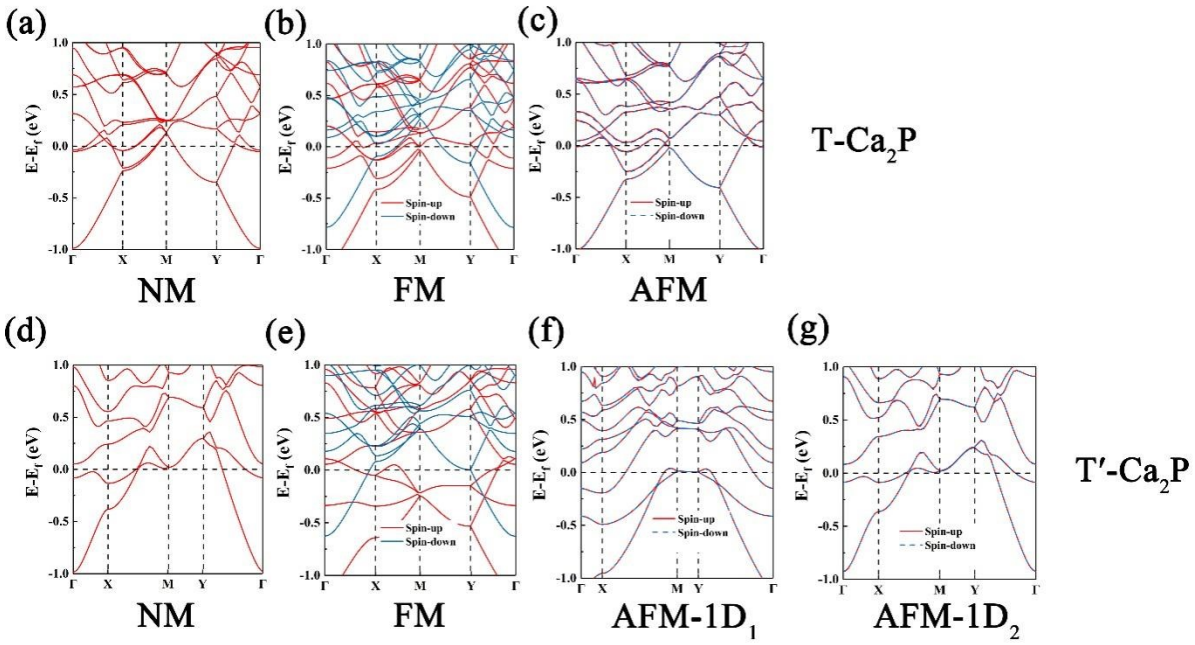

Fig. S4 Calculated band structure of NM FM AFM states of T and T′-Ca_2P.

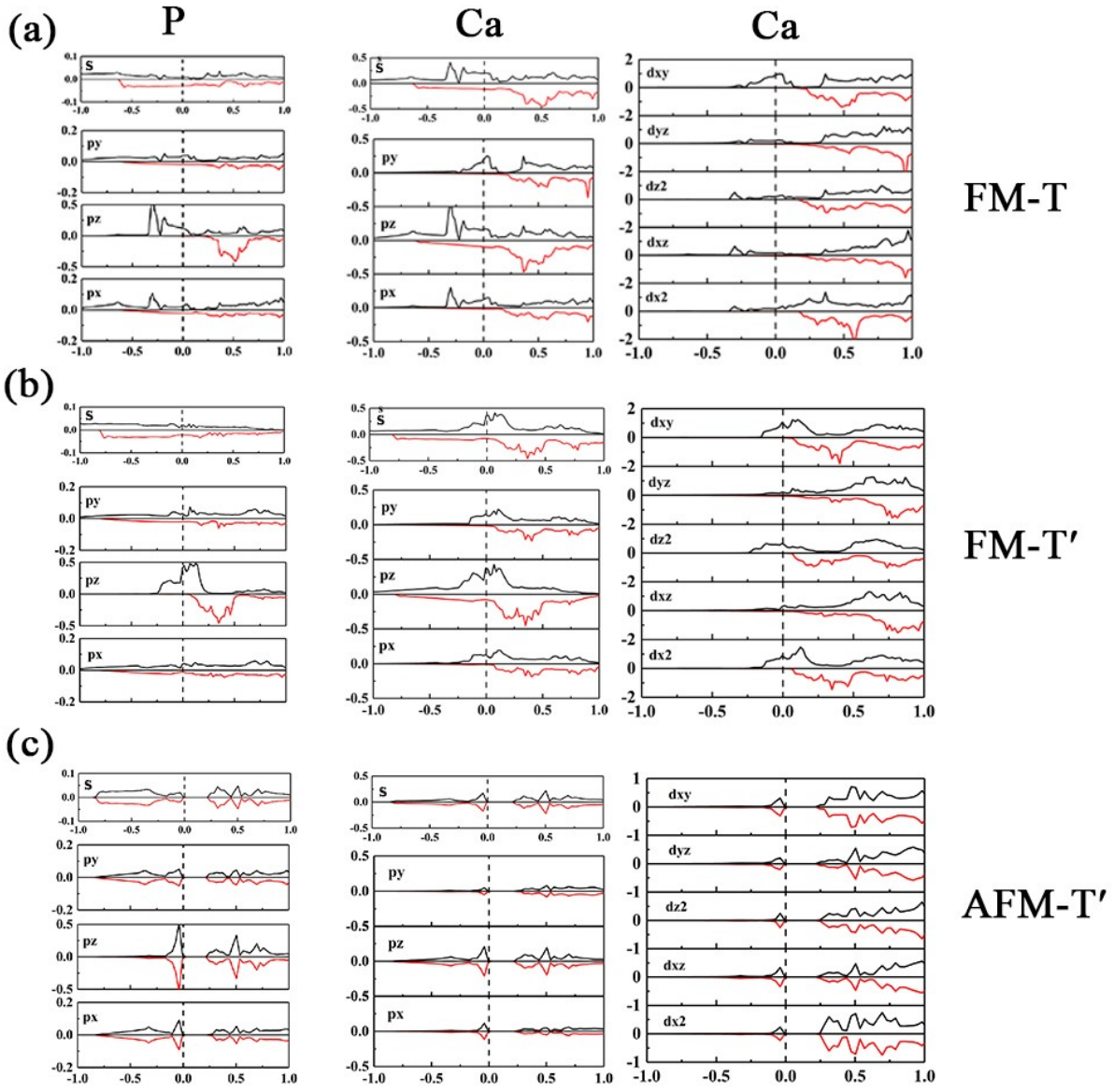

Fig. S5 Calculated PDOS of FM and AFM states of T and T′-Ca_2P.

V. Formation and distribution of electron gas of NM, FM and AFM of T and T′ phases

Confirmation of the formation of electron gas

To investigate the origin of electron gas like behavior as displayed in ELF, three different means are applied. (1st) When one valence electron is removed from $[Ca_2P]^+$, the delocalized ELF features on the surfaces totally disappear, as shown in Fig. S6c†, agreed with previous criterion proposed by Yang *et al*[1]. Therefore, the extra electron transferred from $Ca^{2+}{}_2P^{3-}$ monolayer to form the electron gas. (2nd) From the comparison of the total DOS and partial DOS (as shown in Fig. 1f) of T-Ca_2P and T′-Ca_2P, there is a little contribution from the atomic at fermi level, indicating that the states around E_f are mainly contributed by extra electrons. (3th) The calculated results of spin-polarization show that the magnetic moment within the default atomic radius is only 20% of the total one ($0.26\mu_B/1.32\mu_B$), indicating the magnetism of T′-Ca_2P is mainly contributed from the extra electron[2-3] on the surface of $(Ca_2P)^+$ monolayer. As the calculation shown in Fig. S2 and S6†, the appearance of ELF and spin density are quite similar. Furthermore, when the extra electron is removed, the spin density also totally disappeared, agreed with that the magnetism is mainly contributed from the extra electron. In general, the results of different means utilized here do confirm the formation of electron gas on Ca_2P system.

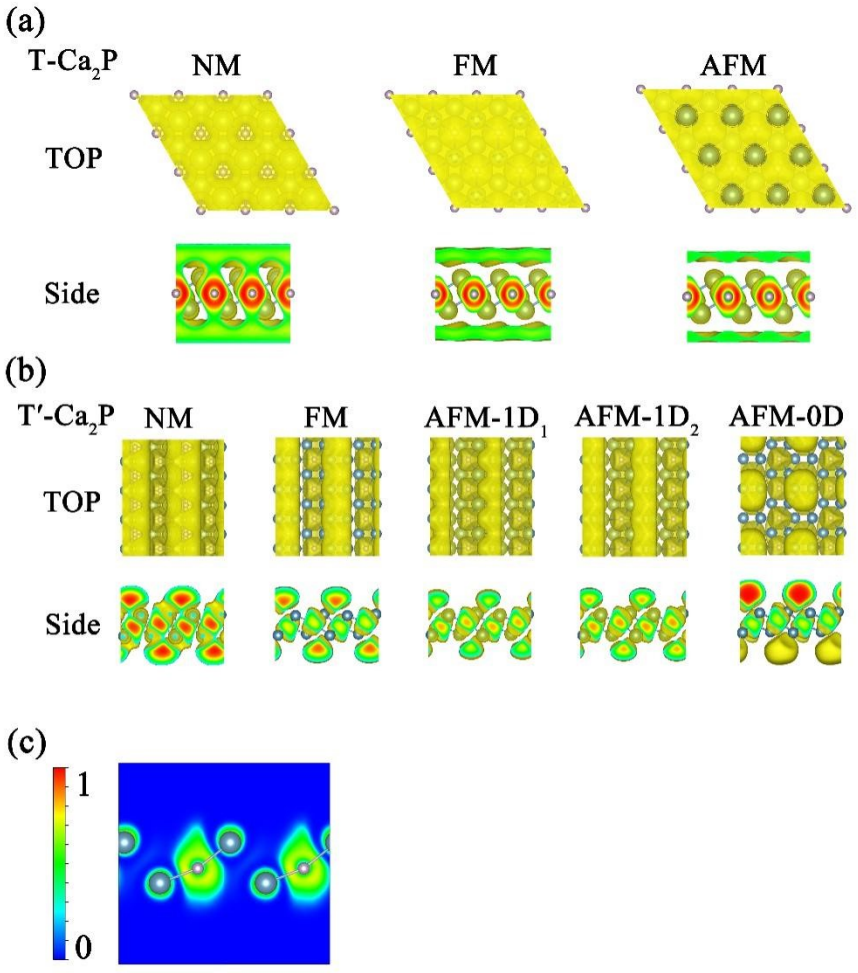

Fig. S6 The ELFs of T-Ca_2P (a) and T′-Ca_2P (b) at different magnetic states, including: NM, FM and AFM T-Ca_2P; NM, FM, AFM-1D_1, AFM-1D_2 and AFM-0D T′-Ca_2P. Isovalue of 0.2 e/Bohr^3. (c) The ELF of $[Ca_2P]^+$ with one valence electron be removed, compared to Ca_2P.

VI. Mechanical properties and interlayer interactions on the structure of T′-Ca_2P.

Equation S1. The in-plane Young's stiffness Y_{2D} of T′-Ca_2P was calculated by the equation as follows:

$$Y_{11} = \frac{C_{11}C_{22} - C_{12}^2}{C_{22}} \quad Y_{22} = \frac{C_{11}C_{22} - C_{12}^2}{C_{11}}$$

where C_{nm} are elastic constants. Y_{11} and Y_{22} are Young's stiffness along direction *a* and direction *b*, respectively.

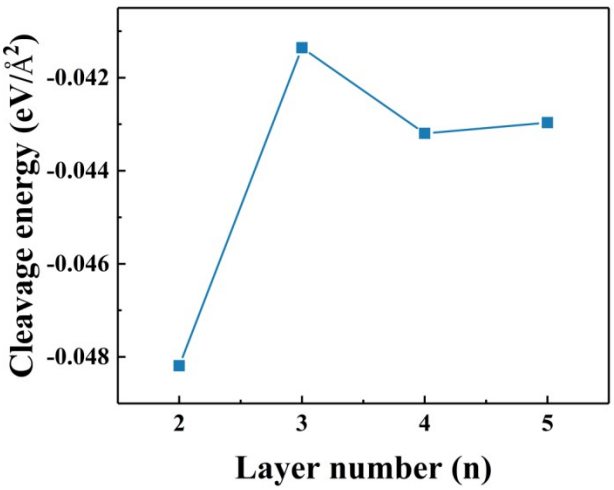

Fig. S7 Calculated cleavage energies of the bilayer to five layers.

VII. Single Na/K atom adsorption

Equation S2. Energy of single M (M= Na/K) atom adsorption was calculated by the equation below:

$$E_{Ads} = E_{M@Ca_2P} - E_{Ca_2P} - E_M$$

where $E_{M@Ca_2P}$ is the total energy of the whole system after K^+ adsorption; E_{Ca_2p} is the total energy of T′-Ca_2P; E_M is energy of a metal atom in bulk.

Equation S3. The charge density difference was estimated by the equation expressed as:

$$\Delta\rho = \rho_{M@Ca_2P} - \rho_{Ca_2P} - \rho_M$$

where $\rho_{M@Ca_2P}$, ρ_{Ca_2P}, ρ_M are the charge densities of the T′-Ca_2P adsorbed metal, the pure T′-Ca_2P and single metal atom, respectively.

Table S2 Adsorption energy, bond length and charge transfer of Na and K adsorbed at T′-Ca_2P.

	Adsorption site	Adsorption energy PBE-GGA/ DFT-D2 (eV)	Distance between Na/K and nearby Ca PBE-GGA/DFT-D2 (Å)	Charge transfer form Na/K PBE-GGA/ DFT-D2 (e)
Na@Ca_2P	S1	-0.19/-0.12	3.74 ~ 3.83/ 3.63~3.75	0.45/0.45
	S2	-0.14/-0.09	3.71 ~ 3.90/ 3.58~3.82	0.41/0.40
	S3	-0.18/-0.13	3,72 ~ 3.85/ 3.58~3.80	0.34/0.33
K@Ca_2P	S1	-0.30/-0.27	4.28 ~ 4.38/ 4.22~4.25	0.51/0.48
	S2	-0.27/-0.21	4.56 ~ 4.07/ 4.05~4.41	0.48/0.43
	S3	-0.31/-0.28	4.14 ~ 4.47/ 3.92~4.56	0.50/0.50

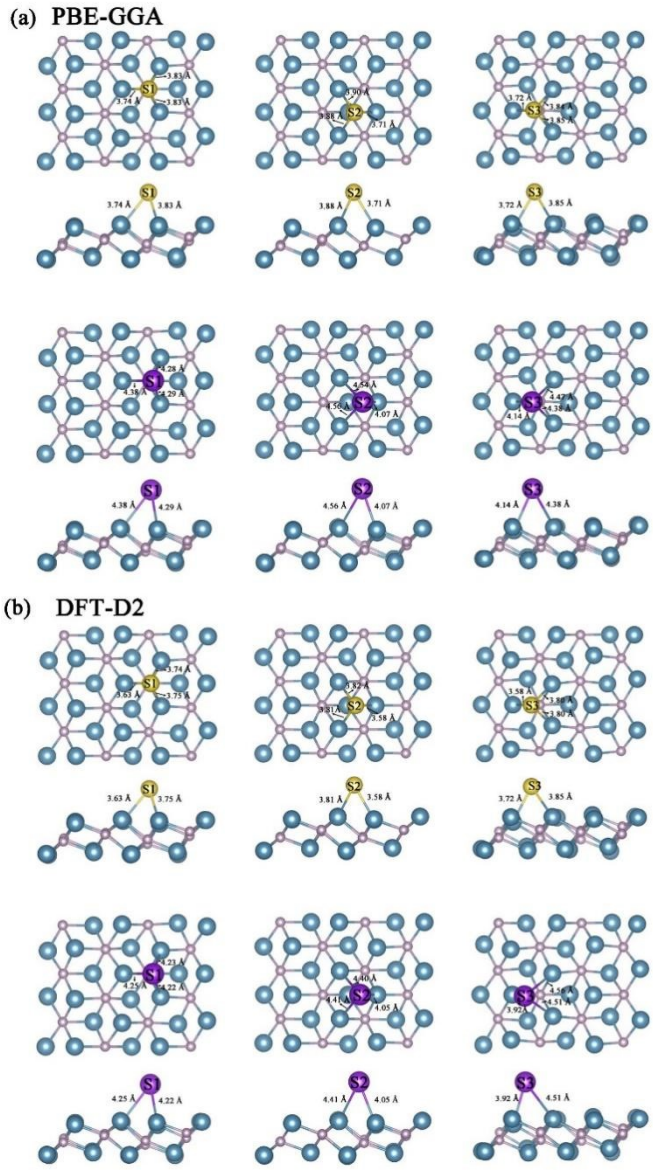

Fig. S8 Top view and side view of Na and K at inequivalent adsorption sites, (a) PBE-GGA method, (b) DFT-D2 method.

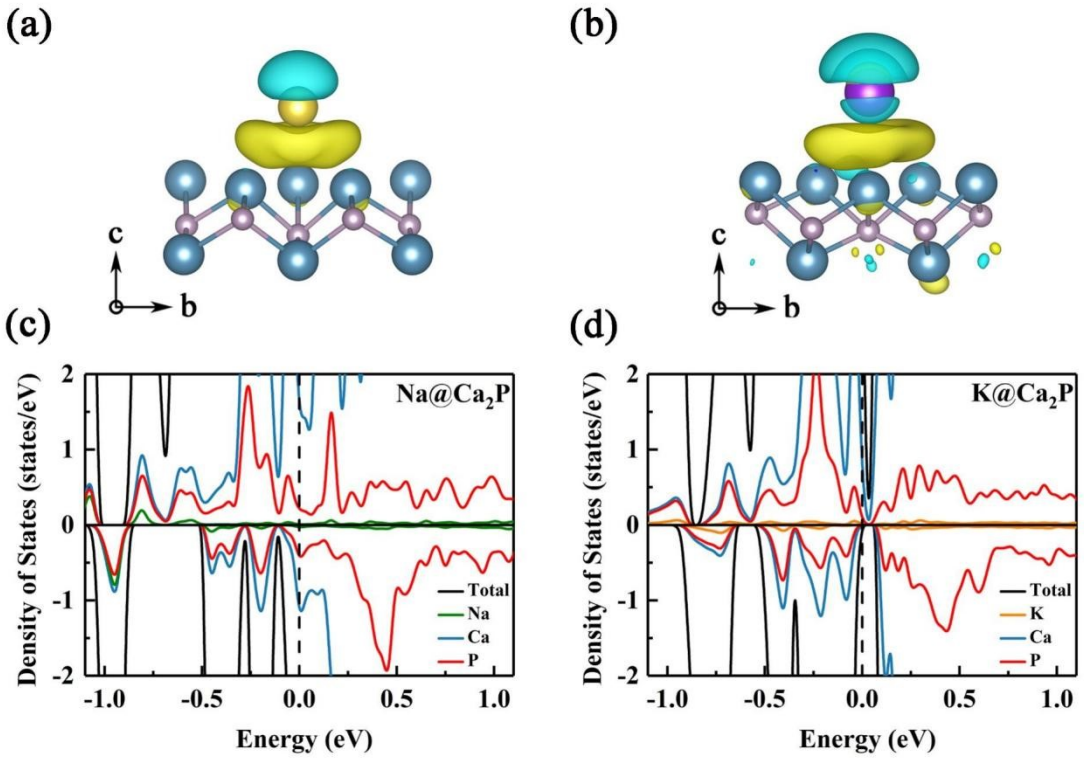

Fig. S9 Charge density difference of Na (a) and K (b) on the favorable sites, respectively (isovalue of 0.05 eÅ^{-3}). Total and projected DOS of Na@Ca_2P (c) and K@Ca_2P (d). The Fermi levels are set to zero, the black dashed line represents the Fermi level.

VIII. Migration rates by incorporation the effects of ZPE and QMT.

The zero-points-energy correction (δE_{ZPE}) to the classical barrier height can be written as[4]

$$\delta E_{ZPE} = \sum_i \frac{h\nu_i^{TS}}{2} - \sum_i \frac{h\nu_i^{IS}}{2}$$

where the first term is the total ZPE of the TS and the second term represent the total ZPE of initial state (IS).

The Wigner zero-point correction to the classical barrier height can be formulated as

$$\delta E_{Wig} = -k_B T \ln\left[\frac{\prod_i sinh(x_i^{IS})/x_i^{IS}}{\prod_i sinh(x_i^{TS})/x_i^{TS}}\right]$$

where $x_i^{IS/TS} = h\nu_i^{IS/Ts}$/2kBT, the ratio of the ZPE to the thermal energy at each vibrational mode. If including the imaginary frequency mode of the product over saddle-point modes along the reaction coordinate in the denominator, the QMT effects on the barrier height are employed through the Wigner tunneling correction.

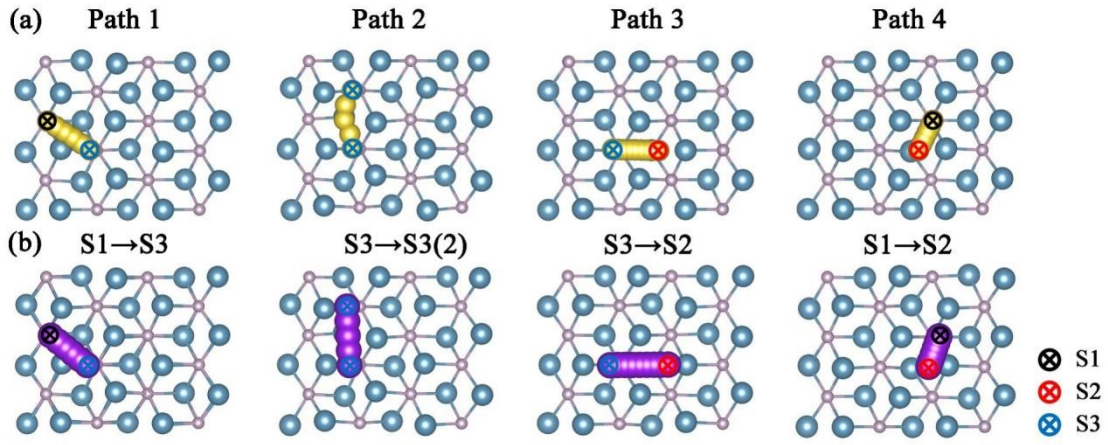

Fig. S10 The migration paths of Na (a) and K (b) diffusion on the T′-Ca_2P monolayer.

IX. Storage capacity of T′-Ca_2P.

Equation S4. The step adsorption energy in each stable Na/K adsorbed phase, as defined by the equation below:

$$E_{step} = \frac{\left[E_{nM@Ca_2P} - E_{mM@Ca_2P} - (n-m)E_M\right]}{n-m}$$

where $E_{nM@Ca_2P}$ and $E_{mM@Ca_2P}$ represents the total energies of the T′-Ca_2P with n and m metal atoms, respectively, E_M is energy of a metal atom in bulk.

Equation S5. The theoretical adsorption capacity of Na/K on T′-Ca_2P was obtained by following equation:

$$C_M = \frac{cxF}{M_{Ca_2P}}$$

where *c* is the number of valence electrons of Na/K (c = 1 for Na/K), *x* is the number of adsorbed M atoms, F is the Faraday constant (26801 mAh·mol^{-1}), and M_{Ca_2P} is the molar weight of the T′-Ca_2P monolayer.

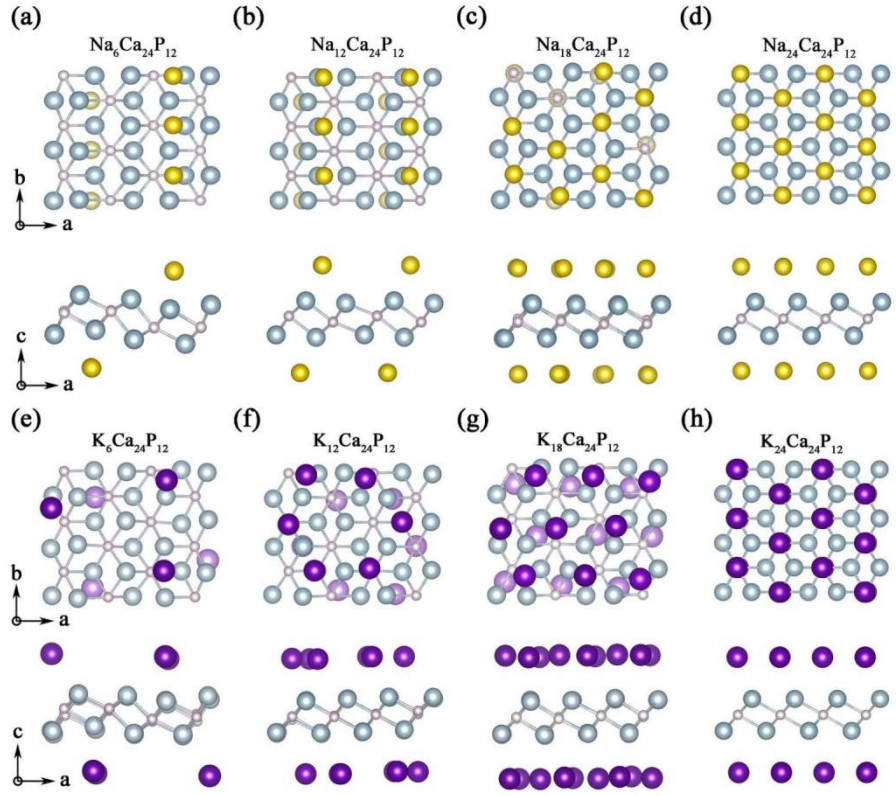

Fig. S11 Optimized structure of Na_xCa_2P (a-d) and K_xCa_2P (e-h) (x=0.5, 1.0, 1.5 and 2.0), respectively.

X. Details of thermodynamic diagram calculations and Structure search by CALYPSO code.

thermodynamic diagram

We assumed that M_2Ca_2P (M = Na/K) can be formed during sodiation and potassiation process, while the chemical potentials of M, Ca and P required to following the thermodynamic equilibrium as:

$$2\Delta\mu_M + 2\Delta\mu_{Ca} + \Delta\mu_P = \Delta H(M_2Ca_2P) \#(1)$$

where $\Delta H(M_2Ca_2P)$ is the formation enthalpy of M_xCa_2P (M = Na/K). To avoid the formation of Ca_2P and NaP (K_2P_3) phases as well as the formation of M, Ca and P crystals, the chemical potentials also satisfy the following constraints:

$$\Delta\mu_{Na} + \Delta\mu_P \leq \Delta H(NaP) \#(2)$$

$$2\Delta\mu_K + 3\Delta\mu_P \leq \Delta H(K_2P_3) \#(3)$$

$$2\Delta\mu_{Ca} + \Delta\mu_P \leq \Delta H(Ca_2P) \#(4)$$

$$\Delta\mu_M \leq 0,\ \Delta\mu_{Ca} \leq 0,\ \Delta\mu_P \leq 0\ \#(5)$$

where $\Delta H(NaP)$ and $\Delta H(K_2P_3)$ are the formation enthalpy of NaP and K_2P_3, respectively. The computed formation entropies of Na_2Ca_2P, K_2Ca_2P, Ca_2P, NaP and K_2P_3 are -2.319, -2.243, -1.944, -0.788 and -2.204 eV, respectively. Using Eq. (1)-(5), the thermodynamic phase diagrams[5-6] of sodiated and potassiated T′-Ca_2P can be obtained.

Structure search by CALYPSO code

The particle-swarm optimization (PSO) scheme, as implemented in the CALYPSO code[7], is employed to search for low energy 2D M_2Ca_2P (M = Na/K), which has been successfully and widely applied in global structure reach for new materials. In our PSO calculations, the population size and the number of generations are set as 30 and 20 (600 different structures), respectively.

The global minimum and the other metastable isomers are shown in Fig. S11. Based on the rank of the structures in order of enthalpy, the global minimum structures for both Na_2Ca_2P and K_2Ca_2P are expected phases in our work, that Na or K evenly distributed on both sides of Ca_2P characterized by 2D "sandwich" structures. These results indicate, for the Na/K-Ca_2P systems, Na and K atoms tend to be adsorbed on the surface of Ca_2P monolayer rather than to destroy the Ca_2P monolayer to form other ternary compounds.

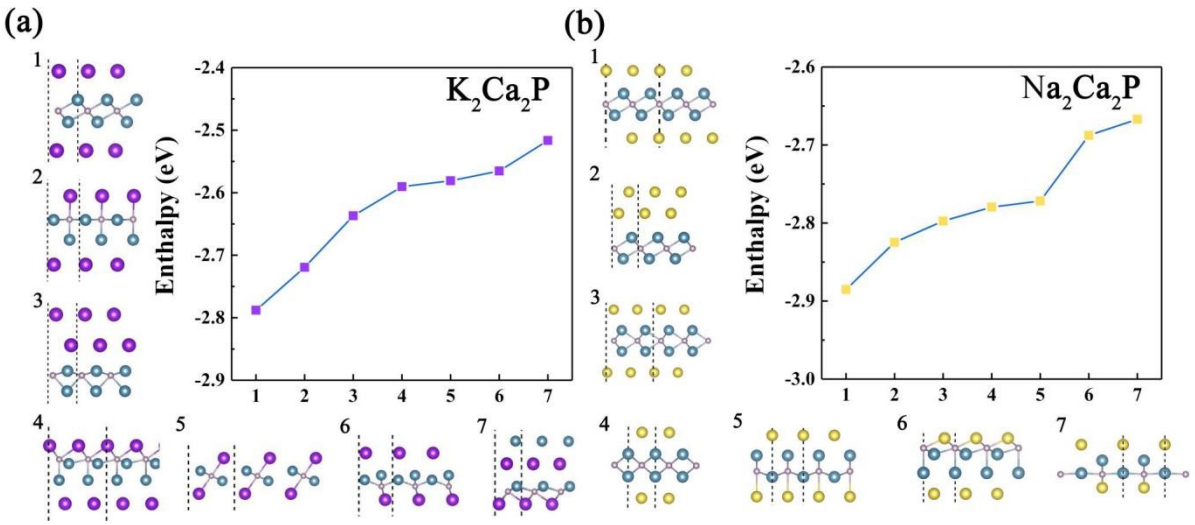

Fig. S12 Isomers of 2D K_2Ca_2P (a) and Na_2Ca_2P (b) found by the Calypso structure search, where insets are the enthalpy of the corresponding structure. The Na, K, Ca and Mg are denoted by yellow, purple, blue and pink spheres, respectively.

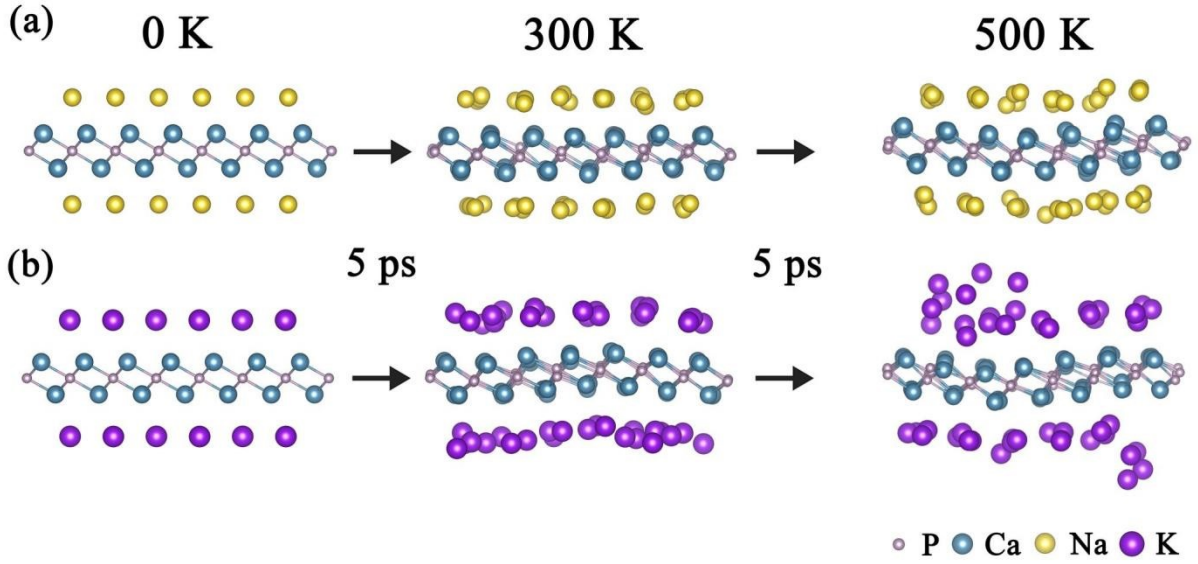

Fig. S13 Snapshots of the structures of (a) Na_2Ca_2P, (b) K_2Ca_2P before and after 5 ps AIMD simulation at 300 K and 500 K, respectively.

XI. Details for formation energy and VOC calculations.

Equation S6. The formation energy of M_xCa_2P at different adsorption content was calculated by the equation:

$$E_f = (E_{M_xCa_2P} - E_{Ca_2P} - xE_M)/(x+1)$$

where $E_{M_xCa_2P}$ is the total energy of T′-Ca_2P with x adsorption number of metal atoms, E_M is energy of a metal atom in bulk.

Equation S7. The average open circuit voltage was calculated by the equation:

$$V_{Ave} = -\frac{\left[E_{nM@Ca_2P} - E_{mM@Ca_2P} - (n-m)E_M\right]}{(n-m)*e}$$

where M_xCa_2P (x = n/m) are the adjacent thermodynamically stable structure with different Na/K ion concentration.

XII. Structural information of M_xCa_2P and ELFs of Na_2Ca_2P and K_2Ca_2P

Table S3 The structure and energies information of M_xCa_2P (M = Na/K x = 0.5 1.0 1.5 2.0), respectively.

structure	E_{step} (eV) PBE-GGA/ DFT-D2	E_f (eV) PBE-GGA/ DFT-D2	L (Å)		Percentage change (%)	
			a PBE-GGA/ DFT-D2	b PBE-GGA/ DFT-D2	a PBE-GGA/ DFT-D2	b PBE-GGA/ DFT-D2
T′-Ca_2P	-	0	14.76/14.70	12.70/12.62	-	-
$Na_{0.5}Ca_2P$	-0.22/-0.24	-0.08/-0.07	14.46/14.33	12.73/12.67	-2.03/-2.48	0.24/0.38
Na_1Ca_2P	-0.08/-0.04	-0.07/-0.07	14.73/14.67	12.68/12.56	-0.20/-0.20	-0.16/-0.44
$Na_{1.5}Ca_2P$	-0.15/-0.18	-0.09/-0.09	14.55/14.41	12.62/12.52	-1.42/-1.97	-0.63/-0.76
Na_2Ca_2P	-0.28/-0.31	-0.13/-0.12	14.53/14.35	12.57/12.45	-1.56/-2.38	-1.02/-1.29

structure	E_{step} (eV) PBE-GGA/ DFT-D2	E_f (eV) PBE-GGA/ DFT-D2	L (Å)		Percentage change (%)	
			a PBE-GGA/ DFT-D2	b PBE-GGA/ DFT-D2	a PBE-GGA/ DFT-D2	b PBE-GGA/ DFT-D2
T′-Ca_2P	-	0	14.76/14.70	12.70/12.62	-	-
$K_{0.5}Ca_2P$	-0.27/-0.27	-0.09/-0.09	14.56/14.46	12.65/12.57	-1.36/-1.65	-0.39/-0.41
K_1Ca_2P	-0.14/-0.15	-0.10/-0.10	14.56/14.46	12.68/12.58	-1.36/-1.63	-0.16/-0.28
$K_{1.5}Ca_2P$	-0.20/-0.22	-0.12/-0.13	14.52/14.43	12.69/12.57	-1.63/-1.80	-0.08/-0.36
K_2Ca_2P	-0.01/-0.09	-0.10/-0.12	15.04/14.93	13.00/12.93	1.90/1.60	2.36/2.45

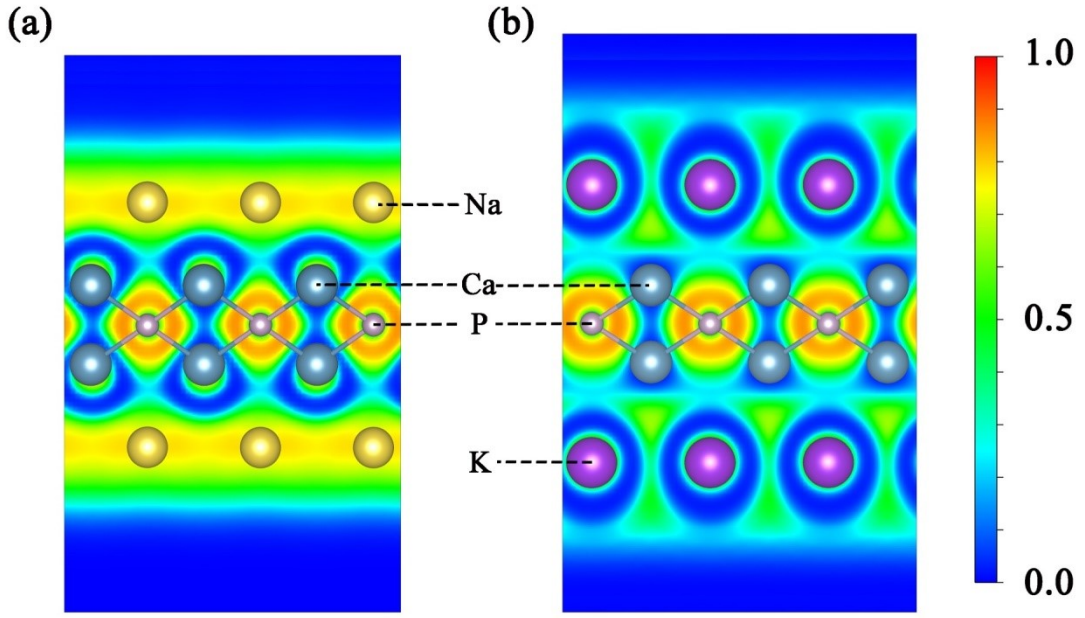

Fig. S14 ELFs of one layer of Na atoms (a) and K atoms (b). The higher value represents the higher electrons localization.

References

1 S. Zhao, Z. Li and J. Yang, *J. Am. Chem. Soc.*, 2014, **136**, 13313-13318.

2 X. Sui, J. Wang, C. Yam and B. Huang, *Nano Lett.*, 2021, **21**, 3813–3819.

3 W. Li, H. Hu and J. Choi, *Phys. Rev. B*, 2021, **103**, 195421.

4 S. Karmakar, C. Chowdhury and A. Datta, J. Phys. Chem. C, 2016, **120**, 14522–14530.

5 T. Zhao, H. Shu, Z. Shen, H. Hu, J. Wang and X. Chen, *J. Phys. Chem. C*, 2019, **123**, 2139-2146.

6 H. Shu, F. Li, C. Hu, P. Liang, D. Cao and X. Chen, *Nanoscale*, 2016, **8**, 2918-2926.

7 Y. Wang, J. Lv, L. Zhu, S. Lu, K. Yin and Q. Li, *J. Phys.: Condens. Matter*, 2015, **27**, 203203.